EUROPEAN ORGANIZATION FOR NUCLEAR RESEARCH (CERN)

CERN-EP-20XX-YYY
LHCb-PAPER-20XX-YYY
March 17, 2019

Measurement of *CP* observables in the process $B^0 \to DK^{*0}$ with two- and four-body D decays

LHCb collaboration[†]

Abstract

Measurements of *CP* observables in $B^0 \to DK^{*0}$ decays are presented, where D represents an admixture of D^0 and $\bar{D}^0$ states. The D is reconstructed in the two-body final states $K^+\pi^-$, π^+K^-, K^+K^- and $\pi^+\pi^-$, and, for the first time, the four-body final states $K^+\pi^-\pi^-\pi^+$, $\pi^-K^+\pi^-\pi^+$ and $\pi^+\pi^-\pi^+\pi^-$. The analysis uses a sample of neutral B mesons produced in proton-proton collisions, corresponding to an integrated luminosity of 3.0 and 1.8 fb^{-1} collected by the LHCb detector in Run 1 and Run 2 of the LHC, respectively. First observations are obtained of the suppressed mode $B^0 \to D(\pi^+K^-)K^{*0}$ and $B^0 \to D(\pi^+\pi^-\pi^+\pi^-)K^{*0}$. The observables are interpreted in terms of the weak-phase γ and associated physics parameters.

[†]Authors are listed at the end of this paper.

1 Introduction

Improved knowledge of the *CP*-violating phase γ (also denoted ϕ_3) is one of the most important goals in flavour physics. This weak phase, which is defined $\gamma \equiv \arg\left(V_{ud}V_{ub}^*/V_{cd}V_{cb}^*\right)$, can be measured through the interference of $b \to c$ and $b \to u$ transitions in tree-level decays. Such a measurement provides a Standard-Model benchmark against which observables determined in loop-mediated processes, expected to be more susceptible to the influence of physics beyond the Standard Model, can be compared.

Current knowledge of γ is dominated by measurements from the LHCb experiment, which together yield $\gamma = (74.0^{+5.0}_{-5.8})^\circ$ [1, 2]. Most of these measurements exploit the decay $B^- \to DK^-$ (unless stated otherwise, charge conjugation is assumed throughout), where D indicates either a D^0 or $\overline{D}^0$ meson reconstructed in a final state common to both. In order to test internal consistency, and to improve overall sensitivity, it is important to augment these measurements with those based on other decay modes, of which $B^0 \to DK^{*0}$, with $K^{*0} \to K^+\pi^-$, is an important example. Both amplitudes contributing to this decay are colour suppressed, in contrast to the charged B-meson case where one of the amplitudes is colour favoured. This attribute leads to a greater suppression of the overall decay rates, but with the benefit of enhanced interference effects.

LHCb has reported studies of $B^0 \to DK^{*0}$ decays using Run-1 data, reconstructing the D meson in the two-body final states $K^\mp\pi^\pm$, K^+K^- and $\pi^-\pi^+$ [3], and also the self-conjugate modes $K^0_S\pi^+\pi^-$ and $K^0_SK^+K^-$ [4, 5]. In addition, the two-body modes $K^-\pi^+$, K^+K^- and $\pi^-\pi^+$ have been exploited in a measurement that analyses the full $B^0 \to DK^-\pi^+$ phase space [6].

In this Letter, results are presented for a study of $B^0 \to DK^{*0}$ decays performed on a data set corresponding to $3.0\,\text{fb}^{-1}$ of integrated luminosity collected at 7 and 8 TeV during Run 1 of the LHC, and $1.8\,\text{fb}^{-1}$ collected at 13 TeV during Run 2 in 2015 and 2016. Observables sensitive to γ and associated parameters are measured for the following final states of the D decay: $K^\mp\pi^\pm$, K^+K^-, $\pi^+\pi^-$, $K^\mp\pi^\pm\pi^+\pi^-$ and $\pi^+\pi^-\pi^+\pi^-$. The study of the two-body modes benefits from several improvements in the analysis with respect to Ref. [3], as well as the larger data set. The four-body modes are analysed for the first time in this decay chain. The measurements involving $D \to \pi^+\pi^-\pi^+\pi^-$ are based on Run-2 data alone, as a suitable selection has not yet been implemented in the offline stripping for Run-1 data.

The Letter is organised as follows. Section 2 presents the observables to be measured, and their relationship to the physics parameters of interest. Section 3 discusses those aspects of the detector, trigger and simulation that are relevant for the measurement. Sections 4, 5 and 6 describe the candidate selection, the fit of the mass spectra and the assignment of systematic uncertainties, respectively. The results, and their interpretation, are given in Sect. 7, and conclusions in Sect. 8.

2 Observables

All observables measured in this analysis have a dependence on γ and three common auxiliary physics parameters. These are the ratio $r_B^{DK^{*0}}$ between the suppressed and favoured B^0 decay amplitudes, expected to be ~ 0.3, the *CP*-conserving strong-phase difference $\delta_B^{DK^{*0}}$ between these amplitudes, and a coherence factor κ, which accounts

for the fact that other amplitudes may contribute to the $B^0 \to DK^+\pi^-$ final state in addition to the two diagrams responsible for the $B^0 \to DK^{*0}$ signal process. Precise definitions of these auxiliary parameters may be found in Ref. [3]. An amplitude analysis of $B^0 \to DK^+\pi^-$ decays has determined the coherence factor to be $\kappa = 0.958^{+0.005}_{-0.046}$ for the kinematic definition of K^{*0} candidates used in this measurement (see Sect. 4) [6], which is close to the limit of unity that would apply if no other contributions were present.

Reconstructing the charm meson through a *CP*-even eigenstate decay, such as $D \to K^+K^-$ or $D \to \pi^+\pi^-$, brings information on γ through a strategy first proposed by Gronau, London and Wyler (GLW) [7, 8]. The asymmetry

$$\mathcal{A}_{CP} \equiv \frac{\Gamma(\bar{B}^0 \to D_{CP}\bar{K}^{*0}) - \Gamma(B^0 \to D_{CP}K^{*0})}{\Gamma(\bar{B}^0 \to D_{CP}\bar{K}^{*0}) + \Gamma(B^0 \to D_{CP}K^{*0})} \tag{1}$$

is measured for both modes, yielding A_{CP}^{KK} and $A_{CP}^{\pi\pi}$, which are expected to be equivalent when very small *CP*-violating effects in the D meson decay are neglected. This asymmetry has the following dependence on the underlying parameters:

$$\mathcal{A}_{CP} \simeq 2\kappa r_B^{DK^{*0}} \sin\delta_B^{DK^{*0}} \sin\gamma, \tag{2}$$

where higher-order terms, including possible corrections from charm mixing and *CP* violation have again been neglected (for clarity, this assumption will apply for the remainder of the discussion).

The charge-averaged rate of decays involving a CP-even D meson is

$$\mathcal{R}_{CP} \equiv 2\frac{\Gamma(\bar{B}^0 \to D_{CP}\bar{K}^{*0}) + \Gamma(B^0 \to D_{CP}K^{*0})}{\Gamma(\bar{B}^0 \to D^0\bar{K}^{*0}) + \Gamma(B^0 \to \bar{D}^0K^{*0})}, \tag{3}$$

which is related to γ and the auxiliary parameters through

$$\mathcal{R}_{CP} \simeq 1 + (r_B^{DK^{*0}})^2 + 2\kappa r_B^{DK^{*0}} \cos\delta_B^{DK^{*0}} \cos\gamma. \tag{4}$$

Experimentally it is convenient to access this parameter by noting that it closely approximates to the observable

$$\mathcal{R}_{CP}^{hh} \equiv \frac{\Gamma(\bar{B}^0 \to D(hh)\bar{K}^{*0}) + \Gamma(B^0 \to D(hh)K^{*0})}{\Gamma(\bar{B}^0 \to D(K\pi)\bar{K}^{*0}) + \Gamma(B^0 \to D(K\pi)K^{*0})} \times \frac{|BF(D^0 \to K^-\pi^+)|}{|BF(D^0 \to h^+h^-)|}, \tag{5}$$

which is measured for both $D \to K^+K^-$ and $D \to \pi^+\pi^-$.

As proposed in Refs. [9, 10], multibody self-conjugate D decays may be used in a quasi-GLW analysis provided their fractional *CP* content is known. Hence the observables $\mathcal{A}_{CP}^{4\pi}$ and $\mathcal{R}_{CP}^{4\pi}$ are measured, which are analogous to the two-body observables defined in Eqs. 1 and 5, but for the decay $D \to \pi^+\pi^-\pi^+\pi^-$. These new observables can be interpreted through equivalent expressions to Eqs. 2 and 4 in which the interference terms acquire a prefactor of $(2F_+^{4\pi} - 1)$, where $F_+^{4\pi}$ is the fractional *CP*-even content of the decay, measured to be 0.769 ± 0.023 from quantum-correlated D decays [11].

The modes $D \to K^\mp\pi^\pm$ are exploited in a method proposed by Atwood, Dunietz and Soni (ADS) [12, 13]. Here, four categories of $B^0 \to DK^{*0}$ decays are possible. Two decays are favoured, and occur when the two final-state kaons have identical charge; these will be designated by the label $K\pi$. The other two decays, labelled πK, involve opposite-charge

kaons and are suppressed. The interference effects, and hence sensitivity to γ, are expected to be significant for the suppressed modes, and negligible for the favoured modes.

The partial-rate asymmetry of the suppressed ADS decays is given by

$$\mathcal{A}^{\pi K}_{\rm ADS} \equiv \frac{\Gamma(\bar{B}^0 \to D(\pi K)\bar{K}^{*0}) - \Gamma(B^0 \to D(\pi K)K^{*0})}{\Gamma(\bar{B}^0 \to D(\pi K)\bar{K}^{*0}) + \Gamma(B^0 \to D(\pi K)K^{*0})} \tag{6}$$

and the charge-averaged rate with respect to the favoured modes by

$$\mathcal{R}^{\pi K}_{\rm ADS} \equiv \frac{\Gamma(\bar{B}^0 \to D(\pi K)\bar{K}^{*0}) + \Gamma(B^0 \to D(\pi K)K^{*0})}{\Gamma(\bar{B}^0 \to D(K\pi)\bar{K}^{*0}) + \Gamma(B^0 \to D(K\pi)K^{*0})}, \tag{7}$$

which have the following dependence on γ and the auxiliary parameters:

$$\mathcal{A}^{\pi K}_{\rm ADS} \simeq 2r_B^{DK^{*0}} r_D^{K\pi} \sin(\delta_B^{DK^{*0}} + \delta_D^{K\pi}) \sin\gamma \tag{8}$$

$$\mathcal{R}^{\pi K}_{\rm ADS} \simeq (r_B^{DK^{*0}})^2 + (r_D^{K\pi})^2 + 2r_B^{DK^{*0}} r_D^{K\pi} \cos(\delta_B^{DK^{*0}} + \delta_D^{K\pi}) \cos\gamma. \tag{9}$$

Here, $r_D^{K\pi} = 0.059 \pm 0.001$ is the ratio between the doubly Cabibbo-suppressed and Cabibbo-favoured decay amplitudes of the neutral charm meson, and $\delta_D^{K\pi} = (194.7^{+8.4}_{-17.6})^\circ$ is a strong-phase difference between these amplitudes [14][1].

In practice, the ratios

$$\mathcal{R}^{\pi K}_{+} = \frac{\Gamma(B^0 \to D(\pi K)K^{*0})}{\Gamma(B^0 \to D(K\pi)K^{*0})} \tag{10}$$

$$\mathcal{R}^{\pi K}_{-} = \frac{\Gamma(\bar{B}^0 \to D(\pi K)\bar{K}^{*0})}{\Gamma(\bar{B}^0 \to D(K\pi)\bar{K}^{*0})} \tag{11}$$

are measured, as these observables are experimentally more robust. The relationships $\mathcal{A}^{\pi K}_{\rm ADS} \simeq (\mathcal{R}^{\pi K}_{-} - \mathcal{R}^{\pi K}_{+})/(\mathcal{R}^{\pi K}_{-} + \mathcal{R}^{\pi K}_{+})$ and $\mathcal{R}^{\pi K}_{\rm ADS} \simeq (\mathcal{R}^{\pi K}_{+} + \mathcal{R}^{\pi K}_{-})/2$ allow the ADS observables to be recovered, where the approximate equalities are exact in the absence of any *CP* violation in the favoured modes.

The ADS method can be extended to the four-body mode $D \to K^\pm\pi^\mp\pi^+\pi^-$. Measurements are made of the observables $\mathcal{R}^{\pi K\pi\pi}_{\pm}$, and from these $\mathcal{R}^{\pi K\pi\pi}_{\rm ADS}$ and $\mathcal{A}^{\pi K\pi\pi}_{\rm ADS}$ are determined, where the definitions are analogous to those of the two-body case. In interpreting the results it is necessary to account for the variation of amplitude across the phase space of the D decay. In the equivalent relations for Eqs. 9 and 8 the amplitude ratio and charm strong-phase difference become $r_D^{K3\pi}$ and $\delta_D^{K3\pi}$, respectively, which are quantities averaged over phase space, and a coherence factor $\kappa_D^{K3\pi}$ enters as a prefactor for the interference terms [15]. These parameters have been measured in charm-mixing and quantum-correlated D-decay studies: $r_D^{K3\pi} = 0.0549 \pm 0.006$, $\delta_D^{K3\pi} = (128^{+28}_{-17})^\circ$ and $\kappa_D^{K3\pi} = 0.43^{+0.17}_{-0.13}$ [16, 17].

Other observables may be studied which are expected to be exhibit negligible *CP*-violation within current experimental sensitivities, but serve as useful controls. In the favoured $K\pi$ and $K\pi\pi\pi$ modes the asymmetries $\mathcal{A}^{K\pi(\pi\pi)}_{\rm ADS} = [\Gamma(\overline{B}^0 \to D(K\pi(\pi\pi))\overline{K}^{*0}) - \Gamma(B^0 \to D(K\pi(\pi\pi))K^{*0}]/[\overline{B}^0 \to D(K\pi(\pi\pi))\overline{K}^{*0} + \Gamma(B^0 \to D(K\pi(\pi\pi))K^{*0}]$ are measured. Also included in this category are observables associated with the decay $B^0_s \to DK^*$. In this case for the ADS selection it is the final state with opposite-sign kaons which

[1] All expressions and charm strong-phase values are given in the convention $CP|D^0\rangle = |\bar{D}^0\rangle$.

constitutes the favoured mode, and so the analogously defined asymmetries $\mathcal{A}_{s,\mathrm{ADS}}^{\pi K(\pi\pi)}$ are measured. Event yields are too small to permit a study of the suppressed mode. Finally, the GLW asymmetries $\mathcal{A}_{s,CP}^{KK}$, $\mathcal{A}_{s,CP}^{\pi\pi}$ and $\mathcal{A}_{s,CP}^{\pi\pi\pi\pi}$ are determined, defined analogously to Eq. 1, and the ratios $\mathcal{R}_{s,CP}^{KK}$, $\mathcal{R}_{s,CP}^{\pi\pi}$ and $\mathcal{R}_{s,CP}^{\pi\pi\pi\pi}$, defined analogously to Eq. 5.

3 Detector, online selection and simulation

The LHCb detector [18, 19] is a single-arm forward spectrometer covering the pseudorapidity range $2 < \eta < 5$, designed for the study of particles containing b or c quarks. The detector includes a high-precision tracking system consisting of a silicon-strip vertex detector surrounding the pp interaction region a large-area silicon-strip detector located upstream of a dipole magnet with a bending power of about 4 Tm, and three stations of silicon-strip detectors and straw drift tubes placed downstream of the magnet. The tracking system provides a measurement of momentum, p, of charged particles with a relative uncertainty that varies from 0.5% at low momentum to 1.0% at 200 GeV/c. The minimum distance of a track to a primary vertex (PV), the impact parameter (IP), is measured with a resolution of $(15 + 29/p_{\mathrm{T}})\,\mu$m, where p_{T} is the component of the momentum transverse to the beam, in GeV/c. Different types of charged hadrons are distinguished using information from two ring-imaging Cherenkov detectors. Photons, electrons and hadrons are identified by a calorimeter system consisting of scintillating-pad and preshower detectors, an electromagnetic calorimeter and a hadronic calorimeter. Muons are identified by a system composed of alternating layers of iron and multiwire proportional chambers.

The online event selection is performed by a trigger, which consists of a hardware stage, based on information from the calorimeter and muon systems, followed by a software stage, which applies a full event reconstruction. Signal events considered in the analysis must satisfy hardware and software trigger requirements. The events used must be triggered at the hardware level when either one of the final state tracks of the signal decay deposits enough energy in calorimeter system, or when one of the other tracks in the event, not reconstructed as part of the signal candidate, fulfils any trigger requirement (*i.e.* mainly events triggered by one high p_{T} muon, hadron, electron or photon coming from a decay of the other B meson produced in the collision). At the software stage, it is required that at least one particle should have a high p_{T} and high χ^2_{IP} where χ^2_{IP} is defined as the difference in the vertex fit χ^2 with and without the inclusion of that particle. A multivariate algorithm is used to identify secondary vertices consistent with being a two-, three- or four-track b decay.

Approximately 2 million simulated events are used to describe the signal shapes and compute efficiencies. In the simulation, pp collisions are generated using Pythia [20] with a specific LHCb configuration [21]. Decays of hadronic particles are described by EvtGen [22], in which final-state radiation is generated using Photos [23]. The interaction of the generated particles with the detector, and its response, are implemented using the Geant4 toolkit [24] as described in Ref. [25].

4 Offline selection

B-meson candidates are built from D and K^{*0} candidates, with the D reconstructed from the seven different decay modes of interest within a $\pm 25\,\text{MeV}$ window around the nominal D^0 mass and the K^{*0} reconstructed from $K^+\pi^-$. K^{*0} candidates are selected from within a $\pm 50\,\text{MeV}$ window around the nominal K^{*0} mass and with a requirement of $|\cos(\theta^*)| > 0.4|$, where the helicity angle θ^* is defined as the angle between the momenta of the K^{*0} daughters in the B-meson rest frame. The B decay chain is refit with the D mass fixed to its nominal value and the D and K^{*0} tracks required to point back to the same vertex.

Gradient Boosted Decision Trees (BDTs) are used to separate signal from combinatorial background. A common BDT is deployed for the favoured and suppressed two-body ADS modes, and similarly for the four-body ADS modes. Three more BDTs are used to select the K^+K^-, $\pi^+\pi^-$ and $\pi^+\pi^-\pi^+\pi^-$ decays. The BDTs are trained with samples of fully simulated events as signal and data events from the upper B mass sideband ($m(B) > 5800\,\text{MeV}$) as background. Both samples are required to have passed the D and K^{*0} mass-window requirements and helicity-angle cut. The discriminating variables in the BDT comprise: the B vertex-fit χ^2; the χ^2_{IP} of the B, D and K^{*0} daughters; the transverse momentum of the K^{*0} daughters; the angle between the B momentum and the vector between the PV and the B decay vertex; and the B p_{T} asymmetry between the B candidate and other tracks from the PV, defined as

$$p_{\text{T}}\text{ asymmetry} = \frac{{p_{\text{T}}}^B - {p_{\text{T}}}^{\text{cone}}}{{p_{\text{T}}}^B + {p_{\text{T}}}^{\text{cone}}}, \tag{12}$$

where ${p_{\text{T}}}^B$ is the transverse momentum of the B candidate and ${p_{\text{T}}}^{\text{cone}}$ is the scalar sum of the transverse momenta of all other tracks in a cone of 1.5 radians surrounding the B candidate. This variable quantifies the isolation of the B candidate. The two-body BDTs also use the p_{T} and χ^2_{IP} of the D daughters. These variables are not included in the four-body BDTs as they depend on the kinematics of the multi-body phase space of the D decay, which is not well known and hence poorly modelled in simulation.

Particle-identification (PID) information from the RICH detectors is used to reconstruct the D decays. This selection is applied such that no candidate can appear in more than one D decay category. A tight PID cut is applied to the K^{*0} daughter kaon to suppress contamination from $B^0 \to D\pi^+\pi^-$ decays, with a pion misidentified as a kaon.

Background from charmless B decays that peaks at the same invariant mass as the signal is suppressed by requiring that the significance of the flight distance of the D candidate be greater then 3σ.

It is possible for both the kaon and pion (or one of two pions, in the four-body case) from the D decay in the favoured mode to be misidentified, and thus pollute the suppressed sample. To eliminate this source of contamination, the D invariant mass is reconstructed with the opposite mass hypothesis for the kaon and pion. Candidates within $\pm 15\,\text{MeV}$ of the nominal D mass in this alternative reconstruction are vetoed.

An additional background can arise from $B^0 \to D^-h^+$ ($h = K, \pi$), $D_s^-K^+$ or $D_s^+\pi^-$ decays, in which a kaon and pion from the charm meson is reconstructed as the K^{*0} candidate. This contamination is removed by imposing a $\pm 15\,\text{MeV}$ veto around the nominal $D^+_{(s)}$ mass in the invariant mass of the relevant three tracks.

Finally, a veto of $\pm 25\,\text{MeV}$ around the nominal B^+ mass in the invariant mass of the D and the K^{*0} daughter kaon is applied. This eliminates backgrounds from $B^+ \to DK^+$ decays combined with a random pion that pollutes invariant masses above the signal region.

5 Invariant mass fit

The selected data set comprises seven D final states and two LHC runs. The sample can be further divided into B^0 and $\overline{B}^0$ candidates, based on the charge of the daughter kaon from the K^{*0} meson. This gives a total of 26 categories, as there are no Run-1 data in the $\pi^+\pi^-\pi^+\pi^-$ channel. The invariant-mass distributions are fit simultaneously in these catgories with an unbinned extended maximum likelihood fit. A fit model is developed using simulated signal and background samples reconstructed as the signal decay and passing the selection requirements. This model contains the following components:

1. $B^0 \to DK^{*0}$ signal decays, described by a Cruijff function with a floating mean and width;
2. $\overline{B}^0_s \to DK^{*0}$ decays, also described by a Cruijff function with a floating mean and width;
3. Combinatorial background candidates, described by an exponential function with a floating slope;
4. Partially reconstructed backgrounds from $B^0 \to D^*K^{*0}$ and $\overline{B}^0_s \to D^*K^{*0}$ decays, with $D^* \to D^0\pi^0$ and $D^* \to D^0\gamma$ where the neutral particle is not reconstructed. These contributions are described by analytic probability distribution functions (PDFs) made up of a parabola convolved with a double Gaussian function, as further described in Ref. [26]. The form of the parabola depends on both the missed particle and the helicity of the D^* and K^{*0}, which can be equal to zero (longitudinal polarisation) or one. Four different shapes are therefore needed to describe these backgrounds;
5. Partially reconstructed background from $B^+ \to DK^+\pi^-\pi^+$ decays, where the π^+ is not reconstructed. This contribution is described by the superposition of two Gaussian functions and a parabola convolved with a double Gaussian;
6. A background from $B^0 \to D\pi^+\pi^-$, with one of the pions misidentified as a kaon, described by a double Crystal Ball shape.

The signal and combinatorial background yields are floated separately for each LHC run. The ratios of the yields of the partially reconstructed backgrounds with respect to the signal yields are assumed to be the same in Run 1 and Run 2. The same assumption cannot be made for the misidentified $B^0 \to D\pi^+\pi^-$ background, as the yield of this background is affected by the efficiency of the PID requirement on the kaon from the K^{*0} candidate, which varies with running period. Simulated signal and background samples are used to determine that the ratio between the yield of this background and the signal yield in Run 2 is expected to be 0.928 ± 0.014 times that in Run 1. This ratio is used as a correction in the fit.

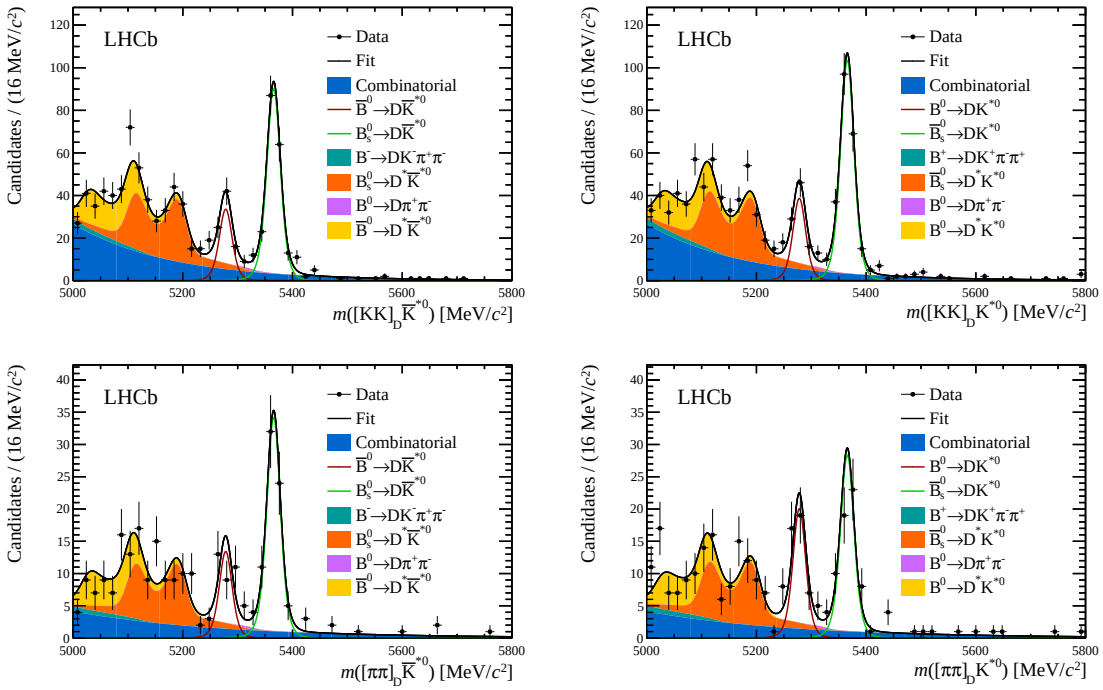

Figure 1: Invariant mass distributions, showing data and fitted invariant-mass model, for the two-body GLW modes. Distributions of (top left) $D(K^+K^-)\bar{K}^{*0}$, (top right) $D(K^+K^-)K^{*0}$, (bottom left) $D(\pi^+\pi^-)\bar{K}^{*0}$ and (bottom right) $D(\pi^+\pi^-)K^{*0}$ invariant masses.

The $B^0 \to D\pi^+\pi^-$ and $\overline{B}{}^0_s \to D^*K^{*0}$ backgrounds are assumed to have no CP asymmetry. Their yields are floated in the ADS modes and fixed in the GLW modes relative to the ADS yields from knowledge of the D^0 branching ratios from Ref. [27] and efficiencies determined from simulation. The $B^0 \to D^*K^{*0}$ background may be sensitive to CP violation, so an asymmetry is allowed in this component, and the yield is floated in each D channel. The relative yields and asymmetries of the $B^+ \to DK^+\pi^-\pi^+$ background are fixed using measurements from Ref. [28].

For both the $B^0 \to D^*K^{*0}$ and $\overline{B}{}^0_s \to D^*K^{*0}$ backgrounds, the proportion of partially reconstructed $D^* \to D^0\gamma$ and $D^* \to D^0\pi^0$ decays is fixed using knowledge of the D^* branching fractions and the relative efficiency as determined from simulation. The fraction of longitudinal polarisation is unknown and is therefore floated in the fit.

Figures 1 to 4 show the invariant mass distributions and functions resulting from the fit. Table 1 gives the signal yields for each D final state. The fit strategy was tested using Monte Carlo toys and was found to be reliable and unbiased for all floated parameters.

The observables introduced in Sect. 2 are determined directly from the fit. The ratios and asymmetries between the raw yields must be corrected for efficiency differences, production asymmetries and detection asymmetries. To obtain the ratios $\mathcal{R}^{hh}$ and $\mathcal{R}^{4\pi}$ the raw ratios must also be normalised with D^0 branching fractions. These corrections are discussed further in Sect. 6.

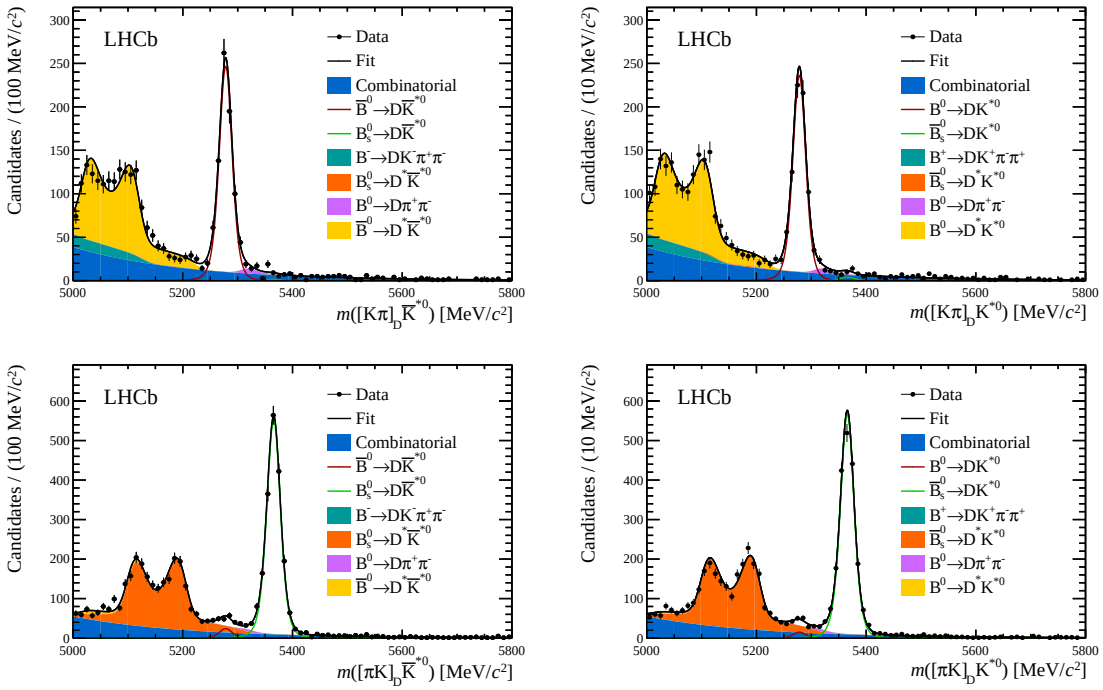

Figure 2: Invariant mass distributions, showing data and fitted invariant-mass model, for the two-body ADS modes. Distributions of (top left) $D(K^-\pi^+)\bar{K}^{*0}$, (top right) $D(K^+\pi^-)K^{*0}$, (bottom left) $D(\pi^+K^-)\bar{K}^{*0}$ and (bottom right) $D(\pi^-K^+)K^{*0}$ invariant masses. The data (black points) and the fitted invariant-mass model (black line) are shown.

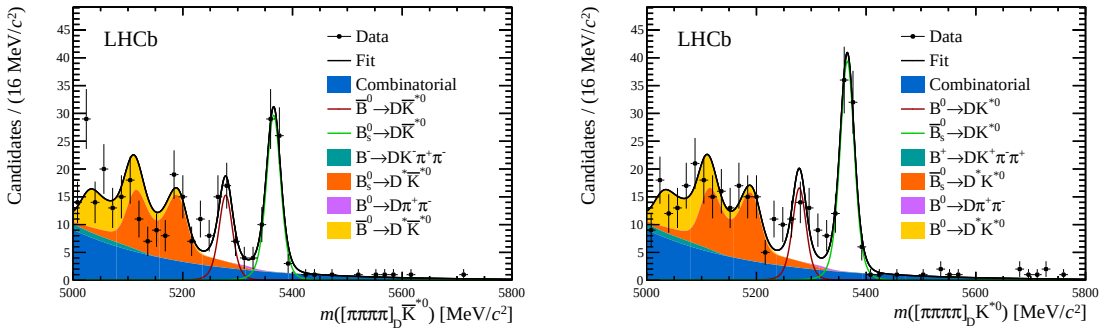

Figure 3: Invariant mass distributions, showing data and fitted invariant-mass model, for the four-body GLW mode. Distributions of (left) $D(\pi^+\pi^-\pi^+\pi^-)\bar{K}^{*0}$, (right) $D(\pi^+\pi^-\pi^+\pi^-)K^{*0}$ invariant masses.

6 Correction factors and systematic uncertainties

The measured observables are either asymmetries, or ratios between similar final states, and are thus inherently robust against systematic biases. Nonetheless small differences in efficiencies between numerator and denominator mean that correction factors must be applied to the ratios, apart from in the case of $\mathcal{R}_{\pm}^{\pi K(\pi\pi)}$ where an identical selection is used for both the suppressed and favoured ADS modes. The selection efficiencies are computed from fully simulated signal samples, which are reweighted in the transverse

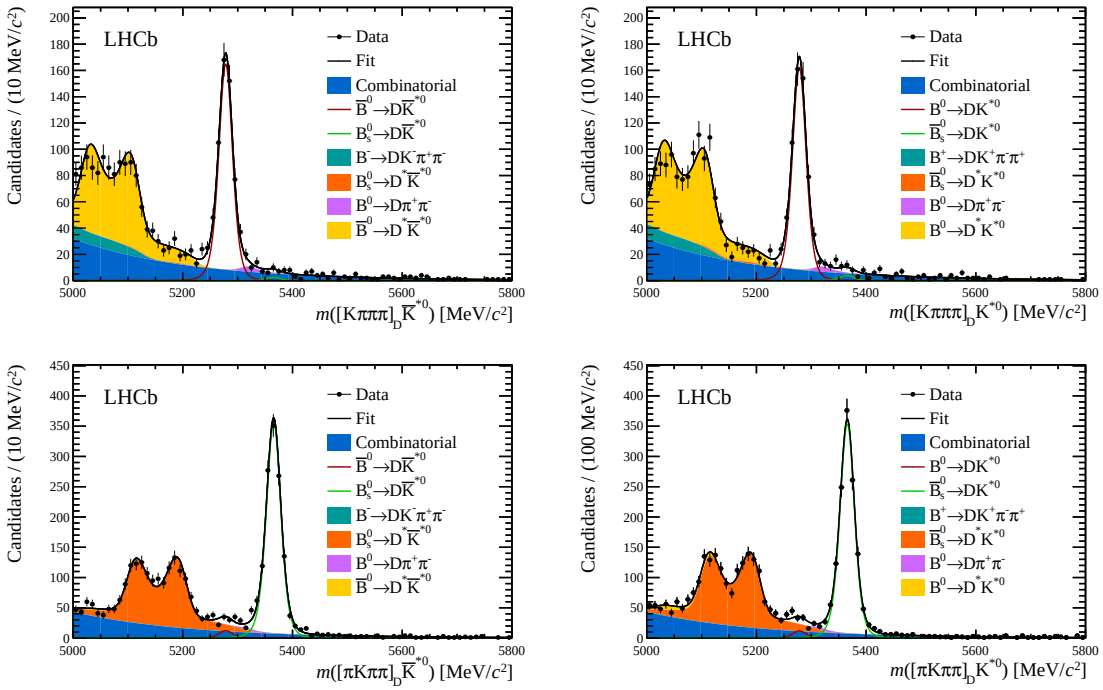

Figure 4: Invariant mass distributions, showing data and fitted invariant-mass model, for the four-body ADS mode. Distributions of (top left) $D(K^-\pi^+\pi^-\pi^+)\bar{K}^{*0}$, (top right) $D(K^+\pi^-\pi^+\pi^-)K^{*0}$, (bottom left) $D(\pi^+K^-\pi^+\pi^-)\bar{K}^{*0}$ and (bottom right) $D(\pi^-K^+\pi^-\pi^+)K^{*0}$ invariant masses.

Table 1: Yields of signal candidates in Run 1 and Run 2. The uncertainties are statistical.

Decay channel	B^0 yield	$\overline{B}^0$ yield
$B^0 \to D(KK)K^{*0}$	67 ± 7	77 ± 8
$B^0 \to D(\pi\pi)K^{*0}$	27 ± 5	40 ± 5
$B^0 \to D(\pi\pi\pi\pi)K^{*0}$	32 ± 7	35 ± 8
$B^0 \to D(K\pi)K^{*0}$	786 ± 24	754 ± 24
$B^0 \to D(\pi K)K^{*0}$	76 ± 12	47 ± 11
$B^0 \to D(K\pi\pi\pi)K^{*0}$	557 ± 21	548 ± 20
$B^0 \to D(\pi K\pi\pi)K^{*0}$	41 ± 10	40 ± 10

momentum and pseudorapidity of the B meson to agree with the data distributions. The efficiencies of the PID requirements are evaluated separately using kinematically selected calibration samples, which are reweighted to match the simulated signal data sets. The PID efficiencies are evaluated separately for B^0 and $\overline{B}^0$ decays and used to correct for asymmetries in the PID requirements. Uncertainties are assigned to account for the finite size of the simulation data sets, the binning schemes used in the reweighting of the calibration sample, and the background-subtraction procedure used for these samples.

As can be seen from Eq. 5, determining $\mathcal{R}_{CP}^{hh}$ requires normalising the measured ratio of yields by a ratio of D^0 branching fractions. The branching ratios are taken from Ref. [27] and the uncertainties propagated through to the observables.

The raw observables are corrected for a detection asymmetry of $(-0.92 \pm 0.20)\%$ in

Run-1 and $(1.0 \pm 0.6)\%$ in Run-2 for each $K^{\pm}\pi^{\mp}$ pair in the final state. The dominant cause of this asymmetry is the shorter interaction length of K^- compared to K^+ mesons. These asymmetries are computed by comparing the charge asymmetries in $D^- \to K^+\pi^-\pi^-$ and $D^- \to K^0_S\pi^-$ calibration samples, weighted to match the kinematics of the kaons and pions in the signal data set.

The observables must also be corrected to account for $A_{\rm prod}$, an asymmetry in the production of B^0 and $\overline{B}^0$ mesons within the acceptance of the analysis. This asymmetry has been measured in bins of B-meson momentum and pseudorapidity in Run-1 [29]. A weighted averaged based on the kinematical distributions of simulated signal events gives $A_{\rm prod} = (-0.8 \pm 0.5)\%$. The same central value is applied for Run 2 with the uncertainty doubled, in order to account for a possible change in assymetry due to the higher collision energy.

Uncertainties are assigned to account for the fixed shape parameters in the invariant-mass model. The fixed tail parameters of the signal shape are assessed as a single source of systematic uncertainty. Uncertainties due to all fixed background shape parameters are assessed simultaneously, apart from those for the partially reconstructed $\overline{B}^0_s \to D^* K^{*0}$ decays, which is an important source of background that overlaps with the signal region. The shape parameters from this important component, which are fully fixed in the fit, are assessed separately.

Other fixed parameters in the fit are the relative proportion of partially reconstructed $D^* \to D^0\pi^0$ and $D^* \to D^0\gamma$ decays, the correction to the relative yield of misidentified $B^0 \to D\pi^+\pi^-$ between Run-1 and Run-2, and the relative yields and CP asymmetries of the partially reconstructed $B^+ \to DK^+\pi^-\pi^+$ background. For the latter, the uncertainties taken from Ref. [28] are doubled to account for the fact that there are possible differences in the phase-space acceptance between the two analyses.

A study is performed of the invariant-mass sidebands of the D candidate in order to search for evidence of any residual charmless background which, if present here, would also contaminate the B signal region. This sideband study is made after imposing the flight distance cut on the D candidate, but without applying the BDT selection, as this may not have a uniform acceptance in D mass. Regions of the sideband are excluded where there are known reflections from D decays with misidentified daughters. No significant signals are found from charmless decays in any mode. The measured yields are extrapolated into the signal region and taken as the central values from which many pseudoexperiments are simulated, and compared with the default result in order to assign a systematic uncertainty.

Table 2 gives the systematic uncertainties for each observable. Systematic uncertainties which are more than two orders of magnitude smaller than the statistical uncertainty are considered to be negligible and ignored. The non-negligible uncertainties are added in quadrature to give the total systematic uncertainty, which in all cases in much smaller than the statistical uncertainty.

The acceptance for the four-body D-decay modes is not fully uniform across phase-space. Studies performed with amplitude models of these decays indicate that, at the current level of sensitivity, this non-uniform acceptance does not lead to any significant bias when the observables are interpreted in terms of the underlying physics parameters.

Table 2: Systematic uncertainties for the observables. Systematic uncertainties more than two orders of magnitude smaller than the statistical uncertainty are neglected. The total systematic uncertainty is calculated by summing all sources in quadrature.

Source	Observable									
	$\mathcal{A}_{CP}^{KK}$	$\mathcal{A}_{CP}^{\pi\pi}$	$\mathcal{R}_{CP}^{KK}$	$\mathcal{R}_{CP}^{\pi\pi}$	$\mathcal{A}_{CP}^{4\pi}$	$\mathcal{R}_{CP}^{4\pi}$	$\mathcal{R}_{+}^{\pi K}$	$\mathcal{R}_{-}^{\pi K}$	$\mathcal{R}_{+}^{\pi K\pi\pi}$	$\mathcal{R}_{-}^{\pi K\pi\pi}$
Statistical	0.10	0.14	0.10	0.19	0.15	0.16	0.021	0.021	0.026	0.025
Selection efficiency	-	-	0.01	0.01	-	0.01	-	-	-	-
PID efficiency	< 0.01	-	< 0.01	< 0.01	< 0.01	0.01	-	-	-	-
Branching ratios	-	-	0.02	0.02	-	0.03	-	-	-	-
Production asymmetry	0.01	0.01	-	-	0.01	-	-	-	-	-
Detection asymmetry	< 0.01	< 0.01	< 0.01	0.01	0.01	0.01	< 0.001	0.001	0.001	0.001
Signal shape parameters	-	-	-	-	-	-	< 0.001	< 0.001	< 0.001	< 0.001
$B_s^0 \to D^* K^{*0}$ shape parameters	-	-	< 0.01	-	-	-	0.001	0.001	0.001	0.001
Other background shape parameters	-	-	-	< 0.01	-	< 0.01	0.001	0.001	0.001	0.002
$D^* \to D^0\gamma/\pi^0$ inputs	-	-	< 0.01	-	-	< 0.01	0.002	0.002	0.002	0.002
$B \to D\pi\pi$ PID correction	-	-	-	-	0.01	-	< 0.001	0.001	-	-
$B \to DK\pi\pi$ inputs	-	-	< 0.01	< 0.01	-	< 0.01	-	-	-	-
Charmless background	0.01	0.01	< 0.01	0.03	0.02	0.01	0.004	0.001	0.002	-
Total systematic	0.01	0.01	0.02	0.04	0.03	0.04	0.005	0.003	0.003	0.003

7 Results and discussion

The measured values for the principal observables are

$$\begin{aligned}
\mathcal{A}_{CP}^{KK} &= -0.051 \pm 0.101 \pm 0.013 \\
\mathcal{A}_{CP}^{\pi\pi} &= -0.182 \pm 0.142 \pm 0.014 \\
\mathcal{R}_{CP}^{KK} &= 0.918 \pm 0.099 \pm 0.020 \\
\mathcal{R}_{CP}^{\pi\pi} &= 1.315 \pm 0.194 \pm 0.040 \\
\mathcal{A}_{CP}^{4\pi} &= -0.026 \pm 0.151 \pm 0.025 \\
\mathcal{R}_{CP}^{4\pi} &= 1.012 \pm 0.165 \pm 0.037 \\
\mathcal{R}_{+}^{\pi K} &= 0.064 \pm 0.021 \pm 0.005 \\
\mathcal{R}_{-}^{\pi K} &= 0.095 \pm 0.021 \pm 0.003 \\
\mathcal{R}_{+}^{\pi K\pi\pi} &= 0.074 \pm 0.026 \pm 0.003 \\
\mathcal{R}_{-}^{\pi K\pi\pi} &= 0.072 \pm 0.025 \pm 0.003,
\end{aligned}$$

where the first uncertainty is statistical, and the second systematic. The values of $R_{\pm}^{\pi K}$ and $R_{\pm}^{\pi K\pi\pi}$ may be used to calculate the ADS observables, which are found to be

$$\begin{aligned}
\mathcal{A}_{\rm ADS}^{\pi K} &= 0.194 \pm 0.186 \pm 0.026 \\
\mathcal{R}_{\rm ADS}^{\pi K} &= 0.080 \pm 0.015 \pm 0.004 \\
\mathcal{A}_{\rm ADS}^{\pi K\pi\pi} &= -0.010 \pm 0.243 \pm 0.018 \\
\mathcal{R}_{\rm ADS}^{\pi K\pi\pi} &= 0.073 \pm 0.018 \pm 0.003.
\end{aligned}$$

All *CP*-asymmetries are compatible with zero. Observables are also determined for the favoured ADS modes, and for the B_s^0 decays. As expected, these are all compatible with the *CP*-conserving hypothesis. Results may be found in Appendix A, together with the results for all observables separated between the Run-1 and Run-2 data sets, and full correlation matrices.

The statistical significances of the signal yields in the previously unobserved channels are calculated using Wilks' theorem [30]. The likelihood profiles are convolved with a Gaussian function of width equal to the systematic uncertainties. This procedure yields a significance of 7.9σ for $B^0 \to D(\pi\pi\pi\pi)K^{*0}$, 5.6σ for $B^0 \to D(\pi K)K^{*0}$ and 4.4σ for $B^0 \to D(\pi K\pi\pi)$, constituting the first observation of the first two modes, and strong evidence for the presence of the suppressed four-body ADS channel.

Put here gammadini interpretation.

8 Conclusion

The measurements of *CP* observables in $B^0 \to DK^{*0}$ decays with D decaying to $K^+\pi^-$, π^+K^-, K^+K^- and $\pi^+\pi^-$ are updated to include LHCb data collected in 2015 and 2016. The results, benefitting from the increased data sample and improved analysis methods, supersede those of the previous study [3]. Measurements with D reconstructed in the $K^+\pi^-\pi^+\pi^-$, $\pi^+K^-\pi^+\pi^-$ and $\pi^+\pi^-\pi^+\pi^-$ final states are presented for the first time. First observations are obtained for the suppressed ADS mode $B^0 \to D(\pi^+K^-)K^{*0}$ and the mode $B^0 \to D(\pi^+\pi^-\pi^+\pi^-)$.

The observables are interpreted in terms of the weak-phase γ and associated parameters add a couple of sentences depending on what is found. Full exploitation of the LHCb Run-2 data set with these modes, and other $B^0 \to DK^{*0}$ decays, will provide powerful constraints on γ, which may be compared to those obtained from studies of other processes.

Acknowledgements

We express our gratitude to our colleagues in the CERN accelerator departments for the excellent performance of the LHC. We thank the technical and administrative staff at the LHCb institutes. We acknowledge support from CERN and from the national agencies: CAPES, CNPq, FAPERJ and FINEP (Brazil); MOST and NSFC (China); CNRS/IN2P3 (France); BMBF, DFG and MPG (Germany); INFN (Italy); NWO (The Netherlands); MNiSW and NCN (Poland); MEN/IFA (Romania); MinES and FASO (Russia); MinECo (Spain); SNSF and SER (Switzerland); NASU (Ukraine); STFC (United Kingdom); NSF (USA). We acknowledge the computing resources that are provided by CERN, IN2P3 (France), KIT and DESY (Germany), INFN (Italy), SURF (The Netherlands), PIC (Spain), GridPP (United Kingdom), RRCKI and Yandex LLC (Russia), CSCS (Switzerland), IFIN-HH (Romania), CBPF (Brazil), PL-GRID (Poland) and OSC (USA). We are indebted to the communities behind the multiple open-source software packages on which we depend. Individual groups or members have received support from AvH Foundation (Germany), EPLANET, Marie Skłodowska-Curie Actions and ERC (European Union), ANR, Labex P2IO, ENIGMASS and OCEVU, and Région Auvergne-Rhône-Alpes (France), RFBR and Yandex LLC (Russia), GVA, XuntaGal and GENCAT (Spain), Herchel Smith Fund, the Royal Society, the English-Speaking Union and the Leverhulme Trust (United Kingdom).

Table 3: Measured observables split by LHC running period.

Observable	Run 1	Run 2
$\mathcal{A}_{CP}^{KK}$	-0.191 ± 0.157 ± 0.008	0.047 ± 0.132 ± 0.024
$\mathcal{A}_{CP}^{\pi\pi}$	-0.061 ± 0.228 ± 0.029	-0.257 ± 0.179 ± 0.013
$\mathcal{R}_{CP}^{KK}$	0.928 ± 0.154 ± 0.026	0.912 ± 0.126 ± 0.021
$\mathcal{R}_{CP}^{\pi\pi}$	1.393 ± 0.326 ± 0.046	1.271 ± 0.237 ± 0.033
$\mathcal{R}_{+}^{\pi K}$	0.045 ± 0.032 ± 0.004	0.076 ± 0.027 ± 0.005
$\mathcal{R}_{-}^{\pi K}$	0.120 ± 0.035 ± 0.005	0.080 ± 0.025 ± 0.003
$\mathcal{R}_{+}^{\pi K\pi\pi}$	0.116 ± 0.045 ± 0.007	0.047 ± 0.031 ± 0.003
$\mathcal{R}_{-}^{\pi K\pi\pi}$	0.099 ± 0.043 ± 0.007	0.056 ± 0.029 ± 0.004
$\mathcal{A}_{\rm ADS}^{K\pi}$	0.034 ± 0.044 ± 0.008	0.055 ± 0.035 ± 0.016
$\mathcal{A}_{\rm ADS}^{K\pi\pi\pi}$	0.029 ± 0.052 ± 0.009	0.042 ± 0.040 ± 0.016
$\mathcal{A}_{s,\rm ADS}^{\pi K}$	0.011 ± 0.027 ± 0.010	0.002 ± 0.022 ± 0.019
$\mathcal{A}_{s,\rm ADS}^{\pi K\pi\pi}$	-0.042 ± 0.035 ± 0.011	0.012 ± 0.026 ± 0.020
$\mathcal{A}_{s,CP}^{KK}$	-0.031 ± 0.078 ± 0.011	0.131 ± 0.070 ± 0.020
$\mathcal{A}_{s,CP}^{\pi\pi}$	-0.058 ± 0.171 ± 0.011	-0.129 ± 0.108 ± 0.020
$\mathcal{R}_{s,CP}^{KK}$	1.140 ± 0.093 ± 0.030	1.006 ± 0.074 ± 0.022
$\mathcal{R}_{s,CP}^{\pi\pi}$	0.826 ± 0.145 ± 0.022	1.222 ± 0.137 ± 0.028

Appendices

A Additional results

The measured values of the observables for the B_s^0 decays and for the ADS asymmetry in the favoured B^0 and B_s^0 modes are as follows:

$$\begin{aligned}
\mathcal{A}_{\rm ADS}^{K\pi} &= 0.047 \pm 0.027 \pm 0.010 \\
\mathcal{A}_{\rm ADS}^{K\pi\pi\pi} &= 0.037 \pm 0.032 \pm 0.011 \\
\mathcal{A}_{s,\rm ADS}^{\pi K} &= 0.006 \pm 0.017 \pm 0.012 \\
\mathcal{A}_{s,\rm ADS}^{\pi K\pi\pi} &= -0.007 \pm 0.021 \pm 0.013 \\
\mathcal{A}_{s,CP}^{KK} &= 0.057 \pm 0.052 \pm 0.011 \\
\mathcal{A}_{s,CP}^{\pi\pi} &= -0.109 \pm 0.092 \pm 0.015 \\
\mathcal{R}_{s,CP}^{KK} &= 1.062 \pm 0.058 \pm 0.018 \\
\mathcal{R}_{s,CP}^{\pi\pi} &= 1.052 \pm 0.100 \pm 0.018 \\
\mathcal{A}_{s,CP}^{4\pi} &= 0.124 \pm 0.085 \pm 0.021 \\
\mathcal{R}_{s,CP}^{4\pi} &= 0.964 \pm 0.0.86 \pm 0.031
\end{aligned}$$

The observables are also measured separately for Run-1 and Run-2; these measurements are presented in Table 3. Correlation matrices for the statistical and systematic uncertainties of the B^0 observables are given in Tables 4 and 5 respectively.

Table 4: Statistical correlation matrix for the measured observables.

	$\mathcal{A}_{CP}^{KK}$	$\mathcal{A}_{CP}^{\pi\pi}$	$\mathcal{R}_{CP}^{KK}$	$\mathcal{R}_{CP}^{\pi\pi}$	$\mathcal{A}_{CP}^{4\pi}$	$\mathcal{R}_{CP}^{4\pi}$	$\mathcal{R}_{+}^{\pi K}$	$\mathcal{R}_{-}^{\pi K}$	$\mathcal{R}_{+}^{\pi K\pi\pi}$	$\mathcal{R}_{-}^{\pi K\pi\pi}$	$\mathcal{A}_{\rm ADS}^{K\pi}$	$\mathcal{A}_{\rm ADS}^{K\pi\pi\pi}$
$\mathcal{A}_{CP}^{KK}$	1.00	0.00	0.03	0.00	0.00	0.00	-0.00	-0.00	0.00	0.00	-0.00	0.00
$\mathcal{A}_{CP}^{\pi\pi}$	0.00	1.00	0.00	0.07	-0.00	0.00	0.00	0.00	-0.00	0.00	0.00	0.00
$\mathcal{R}_{CP}^{KK}$	0.03	0.00	1.00	0.05	0.00	0.04	0.02	0.03	0.01	0.01	-0.00	-0.00
$\mathcal{R}_{CP}^{\pi\pi}$	0.00	0.07	0.05	1.00	0.00	0.03	0.01	0.02	0.01	0.01	-0.00	-0.00
$\mathcal{A}_{CP}^{4\pi}$	0.00	-0.00	0.00	0.00	1.00	0.01	-0.00	-0.00	0.00	-0.00	-0.00	-0.00
$\mathcal{R}_{CP}^{4\pi}$	0.00	0.00	0.04	0.03	0.01	1.00	0.01	0.01	0.02	0.02	-0.00	-0.00
$\mathcal{R}_{+}^{\pi K}$	-0.00	0.00	0.02	0.01	-0.00	0.01	1.00	0.05	0.01	0.01	0.09	-0.00
$\mathcal{R}_{-}^{\pi K}$	-0.00	0.00	0.03	0.02	-0.00	0.01	0.05	1.00	0.01	0.01	-0.12	-0.00
$\mathcal{R}_{+}^{\pi K\pi\pi}$	0.00	-0.00	0.01	0.01	0.00	0.02	0.01	0.01	1.00	0.06	-0.00	0.09
$\mathcal{R}_{-}^{\pi K\pi\pi}$	0.00	0.00	0.01	0.01	-0.00	0.02	0.01	0.01	0.06	1.00	-0.00	-0.09
$\mathcal{A}_{\rm ADS}^{K\pi}$	-0.00	0.00	-0.00	-0.00	-0.00	-0.00	0.09	-0.12	-0.00	-0.00	1.00	0.00
$\mathcal{A}_{\rm ADS}^{K\pi\pi\pi}$	0.00	0.00	-0.00	-0.00	-0.00	-0.00	-0.00	-0.00	0.09	-0.09	0.00	1.00

Table 5: Systematic correlation matrix for the measured observables.

	$\mathcal{A}_{CP}^{KK}$	$\mathcal{A}_{CP}^{\pi\pi}$	$\mathcal{R}_{CP}^{KK}$	$\mathcal{R}_{CP}^{\pi\pi}$	$\mathcal{A}_{CP}^{4\pi}$	$\mathcal{R}_{CP}^{4\pi}$	$\mathcal{R}_{+}^{\pi K}$	$\mathcal{R}_{-}^{\pi K}$	$\mathcal{R}_{+}^{\pi K\pi\pi}$	$\mathcal{R}_{-}^{\pi K\pi\pi}$	$\mathcal{A}_{\rm ADS}^{K\pi}$	$\mathcal{A}_{\rm ADS}^{K\pi\pi\pi}$
$\mathcal{A}_{CP}^{KK}$	1.00	0.72	0.31	-0.65	0.31	-0.36	-0.15	-0.63	-0.67	-0.66	-0.51	-0.46
$\mathcal{A}_{CP}^{\pi\pi}$	0.72	1.00	0.39	-0.77	0.19	-0.33	-0.16	-0.77	-0.79	-0.75	-0.65	-0.60
$\mathcal{R}_{CP}^{KK}$	0.31	0.39	1.00	-0.45	0.09	-0.15	0.00	-0.49	-0.56	-0.54	-0.46	-0.48
$\mathcal{R}_{CP}^{\pi\pi}$	-0.65	-0.77	-0.45	1.00	-0.15	0.32	0.11	0.82	0.81	0.81	0.71	0.68
$\mathcal{A}_{CP}^{4\pi}$	0.31	0.19	0.09	-0.15	1.00	-0.10	-0.02	-0.16	-0.14	-0.20	0.01	0.10
$\mathcal{R}_{CP}^{4\pi}$	-0.36	-0.33	-0.15	0.32	-0.10	1.00	0.05	0.33	0.35	0.37	0.22	0.22
$\mathcal{R}_{+}^{\pi K}$	-0.15	-0.16	0.00	0.11	-0.02	0.05	1.00	0.10	0.12	0.12	0.08	0.06
$\mathcal{R}_{-}^{\pi K}$	-0.63	-0.77	-0.49	0.82	-0.16	0.33	0.10	1.00	0.83	0.81	0.72	0.69
$\mathcal{R}_{+}^{\pi K\pi\pi}$	-0.67	-0.79	-0.56	0.81	-0.14	0.35	0.12	0.83	1.00	0.85	0.75	0.75
$\mathcal{R}_{-}^{\pi K\pi\pi}$	-0.66	-0.75	-0.54	0.81	-0.20	0.37	0.12	0.81	0.85	1.00	0.72	0.69
$\mathcal{A}_{\rm ADS}^{K\pi}$	-0.51	-0.65	-0.46	0.71	0.01	0.22	0.08	0.72	0.75	0.72	1.00	0.72
$\mathcal{A}_{\rm ADS}^{K\pi\pi\pi}$	-0.46	-0.60	-0.48	0.68	0.10	0.22	0.06	0.69	0.75	0.69	0.72	1.00

References

[1] LHCb collaboration, *Update of the LHCb combination of the CKM angle γ*, LHCb-CONF-2018-002.

[2] LHCb collaboration, R. Aaij *et al.*, *Measurement of the CKM angle γ from a combination of LHCb results*, JHEP **12** (2016) 087, arXiv:1611.03076.

[3] LHCb collaboration, R. Aaij *et al.*, *Measurement of CP violation parameters in $B^0 \to DK^{*0}$ decays*, Phys. Rev. **D90** (2014) 112002, arXiv:1407.8136.

[4] LHCb collaboration, R. Aaij *et al.*, *Model-independent measurement of the CKM angle γ using $B^0 \to DK^{*0}$ decays with $D \to K^0_S\pi^+\pi^-$ and $K^0_S K^+K^-$*, JHEP **06** (2016) 131, arXiv:1604.01525.

[5] LHCb collaboration, R. Aaij *et al.*, *Measurement of the CKM angle γ using $B^0 \to DK^{*0}$ with $D \to K^0_S\pi^+\pi^-$ decays*, JHEP **08** (2016) 137, arXiv:1605.01082.

[6] LHCb collaboration, R. Aaij *et al.*, *Constraints on the unitarity triangle angle γ from Dalitz plot analysis of $B^0 \to DK^+\pi^-$ decays*, Phys. Rev. **D93** (2016) 112018, arXiv:1602.03455.

[7] M. Gronau and D. Wyler, *On determining a weak phase from CP asymmetries in charged B decays*, Phys. Lett. **B265** (1991) 172.

[8] M. Gronau and D. London, *How to determine all the angles of the unitarity triangle from $B_(d)^0 \to DK_(S)$ and $B_(s)^0 \to D0$*, Phys. Lett. **B253** (1991) 483.

[9] M. Nayak *et al.*, *First determination of the CP content of $D \to \pi^+\pi^-\pi^0$ and $D \to K^+K^-\pi^0$*, Phys. Lett. **B740** (2015) 1, arXiv:1410.3964.

[10] S. Malde *et al.*, *First determination of the CP content of $D \to \pi^+\pi^-\pi^+\pi^-$ and updated determination of the CP contents of $D \to \pi^+\pi^-\pi^0$ and $D \to K^+K^-\pi^0$*, Phys. Lett. **B747** (2015) 9, arXiv:1504.05878.

[11] S. Harnew *et al.*, *Model-independent determination of the strong phase difference between D^0 and $\bar{D}^0 \to \pi^+\pi^-\pi^+\pi^-$ amplitudes*, JHEP **01** (2018) 144, arXiv:1709.03467.

[12] D. Atwood, I. Dunietz, and A. Soni, *Enhanced CP violation with B —¿ K D0 (anti-D0) modes and extraction of the CKM angle gamma*, Phys. Rev. Lett. **78** (1997) 3257, arXiv:hep-ph/9612433.

[13] D. Atwood, I. Dunietz, and A. Soni, *Improved methods for observing CP violation in $B^\pm \to KD$ and measuring the CKM phase gamma*, Phys. Rev. **D63** (2001) 036005, arXiv:hep-ph/0008090.

[14] Heavy Flavor Averaging Group, Y. Amhis *et al.*, *Averages of b-hadron, c-hadron, and τ-lepton properties as of summer 2016*, arXiv:1612.07233, updated results and plots available at http://www.slac.stanford.edu/xorg/hflav/.

[15] D. Atwood and A. Soni, *Role of charm factory in extracting CKM phase information via $B \to DK$*, Phys. Rev. **D68** (2003) 033003, arXiv:hep-ph/0304085.

[16] LHCb collaboration, R. Aaij *et al.*, *First observation of $D^0 - \overline{D}^0$ oscillations in $D^0 \to K^+\pi^+\pi^-\pi^-$ decays and a measurement of the associated coherence parameters*, Phys. Rev. Lett. **116** (2016) 241801, arXiv:1602.07224.

[17] T. Evans *et al.*, *Improved determination of the $D \to K^-\pi^+\pi^+\pi^-$ coherence factor and associated hadronic parameters from a combination of $e^+e^- \to \psi(3770) \to c\bar{c}$ and $pp \to c\bar{c}X$ data*, Phys. Lett. **B757** (2016) 520, arXiv:1602.07430, [Erratum: Phys. Lett.B765,402(2017)].

[18] LHCb collaboration, A. A. Alves Jr. *et al.*, *The LHCb detector at the LHC*, JINST **3** (2008) S08005.

[19] LHCb collaboration, R. Aaij *et al.*, *LHCb detector performance*, Int. J. Mod. Phys. **A30** (2015) 1530022, arXiv:1412.6352.

[20] T. Sjöstrand, S. Mrenna, and P. Skands, *A brief introduction to PYTHIA 8.1*, Comput. Phys. Commun. **178** (2008) 852, arXiv:0710.3820.

[21] I. Belyaev *et al.*, *Handling of the generation of primary events in Gauss, the LHCb simulation framework*, J. Phys. Conf. Ser. **331** (2011) 032047.

[22] D. J. Lange, *The EvtGen particle decay simulation package*, Nucl. Instrum. Meth. **A462** (2001) 152.

[23] P. Golonka and Z. Was, *PHOTOS Monte Carlo: A precision tool for QED corrections in Z and W decays*, Eur. Phys. J. **C45** (2006) 97, arXiv:hep-ph/0506026.

[24] Geant4 collaboration, J. Allison *et al.*, *Geant4 developments and applications*, IEEE Trans. Nucl. Sci. **53** (2006) 270; Geant4 collaboration, S. Agostinelli *et al.*, *Geant4: A simulation toolkit*, Nucl. Instrum. Meth. **A506** (2003) 250.

[25] M. Clemencic *et al.*, *The LHCb simulation application, Gauss: Design, evolution and experience*, J. Phys. Conf. Ser. **331** (2011) 032023.

[26] LHCb collaboration, R. Aaij *et al.*, *Measurement of CP observables in* $B^\pm \to D^{(*)}K^\pm$ *and* $B^\pm \to D^{(*)}\pi^\pm$ *decays*, arXiv:1708.06370, submitted to Phys. Lett. B.

[27] Particle Data Group, M. Tanabashi *et al.*, *Review of particle physics*, Phys. Rev. D **98** (2018) 030001.

[28] LHCb collaboration, R. Aaij *et al.*, *Study of* $B^- \to DK^-\pi^+\pi^-$ *and* $B^- \to D\pi^-\pi^+\pi^-$ *decays and determination of the CKM angle* γ, Phys. Rev. **D92** (2015) 112005, arXiv:1505.07044.

[29] LHCb collaboration, R. Aaij *et al.*, *Measurement of* B^0, B_s^0, B^+ *and* Λ_b^0 *production asymmetries in* 7 *and* 8 *TeV pp collisions*, Phys. Lett. **B774** (2017) 139, arXiv:1703.08464.

[30] S. S. Wilks, *The large-sample distribution of the likelihood ratio for testing composite hypotheses*, Ann. Math. Stat. **9** (1938) 60.

LHCb collaboration

A. N. Other[1].

[1] *University of nowhere*